

Kinetic and Spectroscopic Characterization of Cluster-Derived Supported Pt–Au Catalysts

Corina Mihut,* Claude Descorme,† Daniel Duprez,† and Michael D. Amiridis*,¹

*Department of Chemical Engineering, College of Engineering and Information Technology, Swearingen Engineering Center, University of South Carolina, Columbia, South Carolina 29208; and †Laboratoire de Catalyse en Chimie Organique, UMR 6503 CNRS, Université de Poitiers, 40 avenue du Recteur Pineau, 86022 Poitiers, France

Received February 5, 2002; revised August 5, 2002; accepted August 6, 2002

Silica-supported bimetallic Pt–Au catalysts prepared via different synthetic routes have been investigated in terms of their structural properties, adsorption of CO, and catalytic activity for the selective catalytic reduction of NO by propylene, the oxidation of propylene in the absence of NO, and the ¹⁶O/¹⁸O homoexchange reaction. Catalysts prepared by incipient wetness impregnation from individual Pt and Au precursors exhibited characteristics very similar to those of monometallic Pt catalysts, indicating that in these cases the presence of Au did not affect the catalytic performance of Pt in any significant way. This behavior is consistent with a model in which the two metals remain segregated due to their miscibility gap, and only Pt participates in the adsorption of CO and the reactions under consideration. In contrast, catalysts prepared from a Pt₂Au₄(C≡C^tBu)₈ organo-bimetallic cluster precursor exhibited different behavior both in terms of CO adsorption and their catalytic activity for the three reactions examined. The combination of the kinetic, spectroscopic, and structural characterization data suggests that in this case Pt and Au remain intimately mixed in the form of Pt–Au bimetallic particles and that the presence of Au in these particles modifies the behavior of Pt. © 2002 Elsevier Science (USA)

Key Words: platinum; gold; synthesis; organometallic clusters; CO adsorption; NO_x reduction; propylene oxidation; homoexchange reaction.

1. INTRODUCTION

Supported bimetallic Pt–Au catalysts are primarily synthesized by impregnation, co-impregnation, and deposition-precipitation methods from individual Pt and Au salts. Phase separation of the two metals and inhomogeneous composition of the resulting bimetallic particles are common problems with this type of catalyst due to the large miscibility gap in the bulk phase between Pt and Au (i.e., between 18 and 97 wt% Pt) (1). Furthermore, the low melting point of Au and, therefore, the increased mobility of the Au atoms at high temperatures results in broad Au particle size distributions and difficulties

in stabilizing Au in a small cluster form when these conventional preparation methods are used (2). Such segregation problems can be resolved, at least in principle, by the use of preformed bimetallic cluster precursors, frequently stabilized by organic ligands. Carbonyl-ligated clusters are preferred precursors for heterogeneous catalysts because of the advantage of the easy removal of the carbonyl groups by thermal treatment (3, 4). However, there are no known bimetallic Pt–Au clusters exclusively ligated by carbonyl groups. In contrast, there are a few examples of phosphine stabilized bimetallic Au-containing clusters (i.e., [Pt(Au(PPh₃)₈](NO₃)₂, [Pt(PPh₃)(AuPPh₃)₆](NO₃)₂, and [Pt(AuPPh₃)₂(PPh₃)₂](NO₃)₂) that have been immobilized and thermally activated on solid supports (5, 6). These clusters have high Au content, and the presence of phosphorous in the ligands represents a potential poison for several reactions. Recently, Chandler *et al.* (7–10) reported the preparation of a supported Pt–Au catalyst from a cluster precursor that exclusively contains acetylide ligands and they concluded that true bimetallic Pt–Au particles can be formed via this synthetic route. These ligands are easily removable at high temperatures.

In this paper, we followed the same synthetic approach and we compared the cluster-derived catalysts to catalysts having the same nominal composition, which were prepared by incipient wetness impregnation from hexachloroplatinic and tetrachloroauric acids. The structure of these catalysts was characterized by transmission electron microscopy (TEM), hydrogen chemisorption, and Fourier transform infrared spectroscopy of adsorbed ¹²CO/¹³CO mixtures. The chemical activity was probed by kinetic studies of the selective catalytic reduction of NO by propylene, the oxidation of propylene in the absence of NO, and the ¹⁶O/¹⁸O homoexchange reaction.

2. EXPERIMENTAL METHODS

2.1. Catalyst Preparation

Monometallic Pt/SiO₂ and Au/SiO₂ catalysts with Pt loadings of 1 or 0.15 wt% and Au loadings of 2 or 0.3% were

¹To whom correspondence should be addressed. Fax: (803) 777-8265. E-mail: amiridis@enr.sc.edu.

prepared by incipient wetness impregnation of the SiO₂ support (Davison Syloid 74; calcined overnight at 500°C prior to impregnation; BET surface area 300 m²/g) with aqueous solutions of hexachloroplatinic (H₂PtCl₆ · xH₂O, Aldrich) and tetrachloroauric acids (HAuCl₄ · 3H₂O, Aldrich). Additionally, bimetallic catalysts containing 1 wt% Pt–2 wt% Au or 0.15 wt% Pt–0.3 wt% Au were prepared by co-impregnation (i.e., in this case both precursors were added in the same impregnation solution) using the same support material and precursors. Following impregnation, these catalysts were dried in vacuum for 2 h at 120°C and calcined in air for 5 h at 500°C.

Cluster-derived catalysts were prepared via a wet-impregnation technique by adsorption of the organometallic Pt₂Au₄(C≡C^tBu)₈ cluster precursor (11) from hexane solution onto the SiO₂ support (Aldrich Davisil SiO₂; calcined overnight at 500°C prior to impregnation; BET surface area 360 m²/g) following the same procedure outlined in previous literature reports (7). The concentration of the cluster solution was adjusted so that the final metal loadings of the bimetallic catalysts obtained were approximately the same as those of the catalysts obtained by co-impregnation. Following impregnation, these catalysts were dried in vacuum for 2 h at 60°C, oxidized at 300°C (temperature ramp 10°C/min) in a flowing 5% O₂/He mixture for 2 h, and finally reduced at 200°C (same temperature ramp) for 1 h in a 5% H₂/He mixture. The different activation protocol was chosen in this case to assure mild removal of the acetylide ligands. The metal loadings of all catalysts used in this study were confirmed with elemental analysis via ICP (Galbraith Laboratories).

2.2. Transmission Electron Microscopy Measurements

In preparation for TEM imaging approximately 15 mg of each sample were finely crushed and dispersed in 3 ml deionized water by ultrasonification for 30 min. A drop of this fine dispersion was deposited on a Cu grid and then dried at 40°C for 5–10 min until the excess water was removed. Samples were then examined using a Hitachi 200-kV microscope. Digital images were recorded at magnifications of approximately 200,000. Particle size distributions were obtained by measuring 200 particles for each sample analyzed, using at least three different micrographs.

2.3. Hydrogen Chemisorption Studies

Pt dispersions were obtained via hydrogen chemisorption at room temperature (Autosorb AS-1 gas sorption system). Prior to these measurements, the samples were reduced *in situ* in flowing H₂ at a temperature of 300°C for 3 h, followed by evacuation at the same temperature for 2 h. The samples were then cooled to 40°C and exposed to H₂ at different pressures. Preselected amounts of H₂ were added to the sample and the volumetric uptake of hydro-

gen at different pressures was recorded as a function of the equilibrium pressure up to monolayer coverage. The monolayer coverage was determined based on the “extrapolation to zero pressure” method, which accounts for and subtracts the amount of physisorbed hydrogen. Measurements performed with the 2% Au sample and with the bare silica support indicated no H₂ uptake in these cases. A stoichiometry of one adsorbed hydrogen atom per Pt surface atom was assumed in the calculations.

2.4. Transmission Fourier-Transform Infrared Spectroscopy (FTIR) of Adsorbed CO

Transmission FTIR spectra were collected in the single-beam mode with a resolution of 2 cm⁻¹ using a Nicolet 740 FTIR spectrometer equipped with an MCT-B detector. A 10-cm-long stainless steel IR cell, with NaCl windows cooled by flowing water, was used to collect *in situ* spectra. A heating element wrapped around the cell allowed spectra collection at elevated temperatures. The cell temperature was monitored by a thermocouple placed in close proximity to the catalyst sample. Reference spectra of the clean surfaces in He, 5% H₂/He or 5% O₂/He mixtures were collected at different temperatures as needed. Difference spectra between the samples and the corresponding reference are shown in this paper. Catalyst samples were self-supported wafers with a diameter of 12 mm and a thickness of approximately 20 mg/cm².

Two sets of experiments, each with different activation protocols, were conducted with each catalyst sample. In the first set (i.e., “oxidized” samples) the catalysts were exposed for 2 h in a flowing 5% O₂/He mixture at 300°C (cluster-derived samples) or 400°C (all other samples). In the second set (i.e., “reduced” samples) the catalysts were exposed for 2 h in a flowing 5% H₂/He mixture at 300°C. Following these pretreatments the samples were cooled in either O₂/He or H₂/He mixtures to 100°C, flushed with He, and cooled in He to room temperature. At room temperature a flowing CO/He mixture (CO concentrations of 3000 ppm and 3%) was introduced to the cell and spectra were collected at different time intervals until steady state was reached (usually after 20 min). Helium was then purged through the cell and spectra were collected at different time intervals and elevated temperatures until the entire amount of adsorbed CO was removed from the surface.

Experiments were also conducted at room temperature with mixtures of ¹²CO and ¹³CO at a total flow rate of 5 ml/min and at different ratios (35% ¹²CO–65% ¹³CO, 50% ¹²CO–50% ¹³CO, 65% ¹²CO–35% ¹³CO). The CO in this case was diluted in 95 ml/min of He and was flowed over the catalyst pellet for 30 min to allow equilibration of the surface. The gas-phase spectra of the ¹²CO–¹³CO mixtures were subtracted from the spectra shown in this paper.

2.5. Activity Measurements

2.5.1. $^{16}\text{O}/^{18}\text{O}$ homoexchange reaction. Activity measurements for the $^{16}\text{O}/^{18}\text{O}$ homoexchange reaction were carried out on 20-mg samples in a batch recirculation reactor described in detail elsewhere (12). Prior to reaction, the samples were oxidized at 400°C (10°C/min) in pure $^{16}\text{O}_2$ for 15 min, outgassed under vacuum at 400°C for 15 min, reduced at the same temperature for 15 min in pure H_2 , and finally outgassed again at 400°C under vacuum for 30 min. Following this pretreatment the samples were cooled to the reaction temperature and an equimolar mixture of $^{18}\text{O}_2$ and $^{16}\text{O}_2$ ($P_{\text{total}} = 50$ mbar) was introduced to the reactor. The progress of the reaction was followed by mass spectrometry. Masses 36 ($^{18}\text{O}_2$), 34 ($^{18}\text{O}^{16}\text{O}$), 32 ($^{16}\text{O}_2$), 28 (N_2), and 18 (H_2O) were monitored continuously. (Masses 28 and 18 were monitored to assure that no leak occurred into the reactor.)

The homoexchange reaction rate (V_q), expressed in oxygen atoms exchanged per hour per surface Pt site was calculated as follows:

$$V_q = \frac{2 \cdot MW_{\text{Pt}}}{m \cdot x(\text{wt}) \cdot D \cdot R} \cdot \left(\frac{V_r}{T_r} + \frac{V_c}{T_c} \right) \cdot \left(\frac{dP_{^{18}\text{O}^{16}\text{O}}^0}{dt} \right) \quad [1]$$

where MW_{Pt} is the atomic weight of Pt (g/mol), m is the sample mass (g), x (wt) is the Pt loading of the sample, D is the Pt dispersion, R is the ideal gas constant (8.314 J K⁻¹ mol⁻¹), V_r and V_c are the reactor and loop volumes (cm³), T_r and T_c are the reactor and loop temperatures (K), and $\frac{dP_{^{18}\text{O}^{16}\text{O}}^0}{dt}$ is the initial rate of formation of $^{18}\text{O}^{16}\text{O}$.

2.5.2. Selective catalytic reduction of NO by C_3H_6 . Steady-state activity measurements of the selective catalytic reduction of NO by C_3H_6 (HC-SCR) were conducted in a quartz single-pass fixed-bed flow reactor. Prior to the activity measurements all catalyst samples were oxidized *in situ* at 500°C in a 5% O_2/He mixture for 2 h. Certified mixtures of 1.00% NO in He, 1.03% C_3H_6 in He, 9.80% O_2 in He, and a 99.999% He carrier gas, provided and certified by National Specialty Gases, were used to prepare the reacting gas mixture. Typical gas concentrations used were 1000 ppm_v NO, 1000 ppm_v C_3H_6 , 1% O_2 , and balance helium. Inlet and outlet gas streams were analyzed by the use of a gas chromatograph (Hewlett-Packard 5890) equipped with a thermal conductivity detector and three chromatographic columns: Molecular Sieve 5A (for the analysis of N_2), Porapak Q (for the analysis of N_2O and CO_2), and Graphpac GC (for the analysis of C_3H_6) connected in parallel. The reaction temperature was varied between 200 and 500°C and was monitored by a thermocouple placed in the catalyst bed.

Measurements with samples containing 1% Pt and/or 2% Au used 100 mg of the catalyst in the form of 60/80 mesh particles. The total volumetric flow rate of the reactant mix-

ture was held at 200 cm³/min (1 atm, 25°C) with a corresponding gas hourly space velocity (GHSV) of 120,000 cm³/gm/hr. Measurements with samples containing 0.15 wt% Pt and/or 0.3 wt% Au used 300 mg of catalyst and a total flow rate of 100 cm³/min, so that the overall space velocity was decreased proportionally to the Pt loading and similar overall NO conversions were obtained with both sets of samples. The percentage NO reduction was calculated from the amounts of N_2 and N_2O formed, while the selectivity toward N_2 and N_2O was defined as the amount of N_2 formed divided by the total N_2 and N_2O formed. The only reaction products observed from the oxidation of C_3H_6 were CO_2 and H_2O , and the carbon mass balance was closed within ±5%.

3. RESULTS

3.1. TEM Measurements and H_2 Chemisorption

Number-average metal particle sizes, as well as the results of the hydrogen uptake measurements for different fresh and “used” (i.e., exposed to HC-SCR conditions) samples are summarized in Table 1. Furthermore, metal particle size distributions for the 1Pt and the 1Pt–2Au samples prepared by impregnation, and the cluster-derived 0.5Pt₂Au₄ sample are shown in Fig. 1. The results indicate similar metal particle size averages for the monometallic 1Pt and the co-impregnated 1Pt–2Au samples. In contrast, a smaller average metal particle size (3.4 versus 4.6 nm) and a more narrow distribution are observed with the cluster-derived 0.5Pt₂Au₄ sample. Evidence that mild sintering is taking place as a result of exposure to HC-SCR reaction conditions becomes apparent when the average metal particle sizes of the used samples are compared to the corresponding averages for the fresh samples (Table 1). The observed changes, however, are similar for all three samples and indicate that the cluster-derived 0.5Pt₂Au₄ catalyst maintains a smaller average metal particle size than the other two samples during exposure to temperatures up to 500°C in the presence of O_2 (i.e., HC-SCR conditions). Finally, Pt dispersions estimated based on hydrogen uptake measurements (Table 1) are consistent with the TEM measurements, indicating a higher uptake for the cluster-derived 0.5Pt₂Au₄ sample and mild sintering for the used samples.

TABLE 1

Properties of Different Catalysts Used in this Study

Catalyst	Loading (%)		Average metal particle size (nm)		Hydrogen uptake (moles H_2 /mole Pt)	
	Pt	Au	Fresh	Used	Fresh	Used
1Pt	1.04	—	4.7	5.3	0.158	0.108
1Pt–2Au	0.79	1.81	4.6	5.6	0.153	0.101
0.5Pt ₂ Au ₄	0.77	1.54	3.4	4.0	0.223	0.2

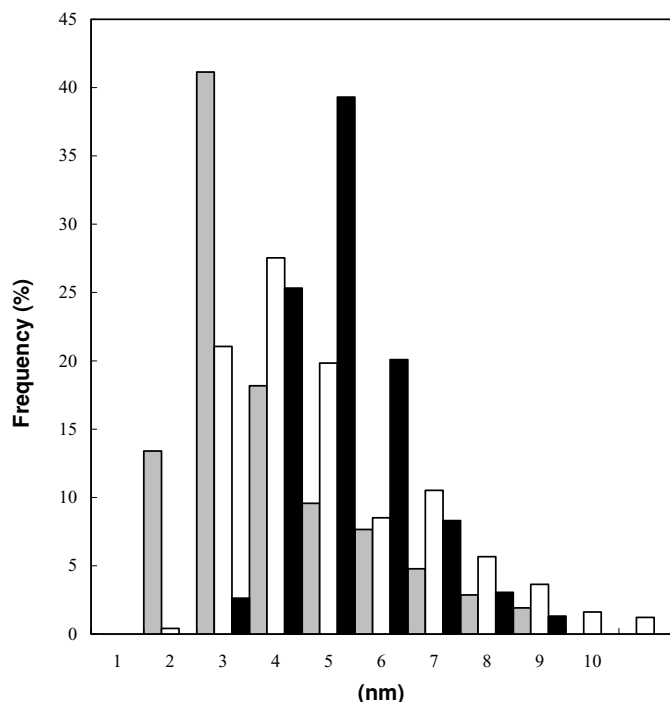


FIG. 1. TEM histograms of the fresh co-impregnated and cluster-derived catalysts (\square , 0.5Pt₂Au₄ fresh sample; \blacksquare , 1Pt fresh sample; \square , 1Pt-2Au fresh sample).

3.2. FTIR Spectroscopy of Adsorbed CO

FTIR studies of adsorbed CO were performed on both reduced and oxidized samples, in an attempt to understand the effect of the Au presence on the structure and properties of Pt. Spectra collected at room temperature on reduced catalyst samples following exposure to 3.3 kPa of CO are shown in Fig. 2. A strong peak at 2070 cm⁻¹ (Fig. 2, spectrum b) is observed in the spectrum of the monometallic 1Pt sample, in agreement with literature reports (13). This peak was assigned to CO linearly adsorbed on fully reduced Pt sites. The addition of Au via co-impregnation, as in the 1Pt-2Au sample, did not affect the CO adsorption (Fig. 2, spectrum c), consistent with previous literature reports (7, 13, 14). Furthermore, no peak assignable to CO adsorbed on Au was observed for the 2Au sample (Fig. 2, spectrum d).

In contrast, some significant differences can be noticed in the spectra of the 0.5Pt₂Au₄ catalyst (Fig. 2, spectrum a) in agreement with similar results reported by Chandler *et al.* (7) for the adsorption of CO on cluster-derived Pt-Au catalysts. In particular, a red shift from 2070 to 2064 cm⁻¹ is observed in the position of the peak assigned to CO linearly bound to Pt, and a new peak is observed at 2117 cm⁻¹ assigned to CO bound to finely dispersed Au. Furthermore, a weak shoulder and substantial asymmetric tailing in the low-frequency region can be observed in the CO-Pt peak of Fig. 2, spectrum a. Similarly, substantial asymmetric tail-

ing in the high-frequency region can be observed in the CO-Au peak of the same spectrum. These features are more pronounced than the corresponding asymmetric tailing observed in the spectra of the monometallic Pt/SiO₂ and the co-impregnated Pt-Au/SiO₂ samples (Spectra 2c and 2b) and suggest that the cluster-derived catalyst contains a broader distribution of CO adsorption sites of different adsorption strengths. Indeed, attempts to deconvolute these peaks using different software packages, yielded results indicating that a number of smaller intensity peaks is needed in order to fit the asymmetric tailing shown in Fig. 2, spectrum a.

Purging the CO-saturated 0.5Pt₂Au₄ sample with an inert atmosphere results in the complete removal of the Au-bound CO (Fig. 3) after approximately 40 min. At the same time, the peak at 2064 cm⁻¹ assigned to Pt-bound CO decreases slightly in intensity at room temperature and is completely eliminated at temperatures around 150°C. These results are in agreement with results from previous studies on supported Au and Pt-Au catalysts, where outgassing at room temperature completely depletes the band associated with CO bound to Au (15-17).

Spectra of adsorbed CO on a "used" catalyst following a reduction treatment at 300°C are shown in Fig. 4. Even after exposure to reaction conditions the two distinctive IR features (namely, the red shift in the CO-Pt peak and the appearance of the CO-Au peak) are still present. This result is consistent with the kinetic results, indicating no catalyst deactivation or change in the selectivity toward N₂ even after prolonged exposure of the 0.5Pt₂Au₄ catalyst to the reaction conditions. Similar to the fresh

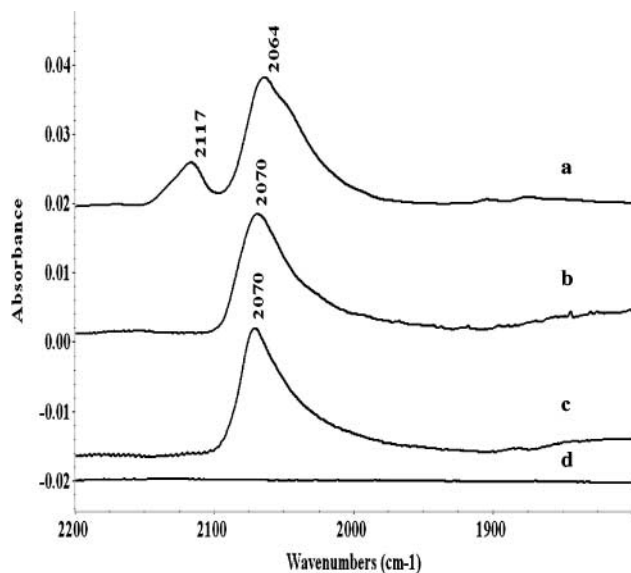


FIG. 2. IR spectra of adsorbed CO at room temperature (30°C) on reduced SiO₂-supported Pt and Pt-Au catalysts. Spectra were collected immediately following the removal of gas-phase CO: (a) 0.5Pt₂Au₄, (b) 1Pt, (c) 1Pt-2Au, (d) 2Au.

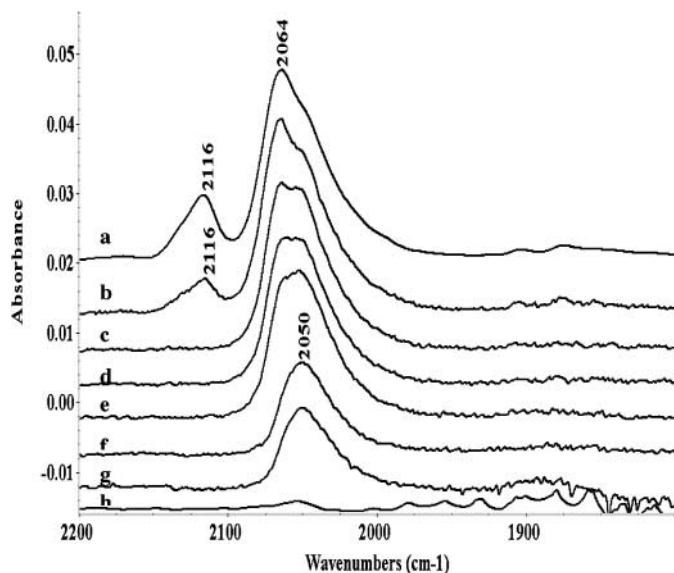


FIG. 3. IR spectra of adsorbed CO on reduced $0.5\text{Pt}_2\text{Au}_4$ catalyst. Spectra were collected following exposure to 0.3 kPa CO for 1 h at room temperature (RT) and He purge: (a) immediately following CO gas-phase removal at RT, (b) for 5 min at RT, (c) for 70 min at RT, (d) for 230 min at RT, (e) for 10 min at 50°C , (f) for 10 min at 75°C , (g) for 10 min at 100°C , and (h) for 10 min at 150°C .

cluster-derived sample, purging with He at room temperature quickly removed the CO–Au peak, while an elevated temperature was required for the elimination of the CO–Pt peak.

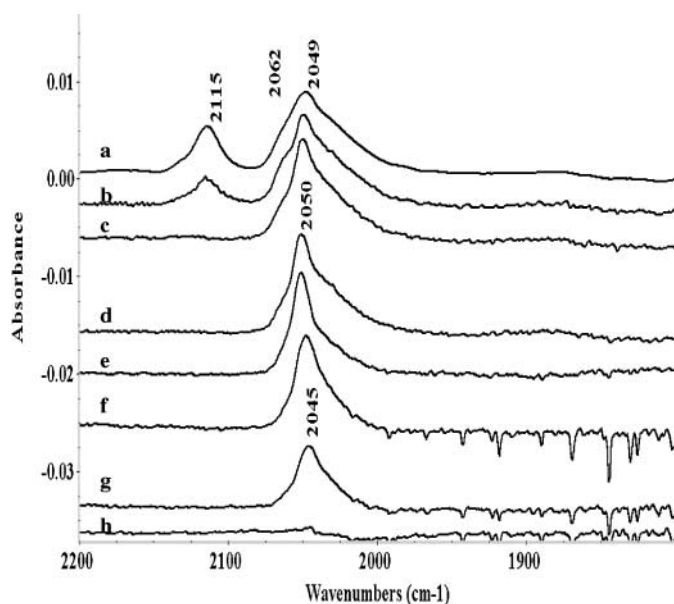


FIG. 4. IR spectra of adsorbed CO on used reduced $0.5\text{Pt}_2\text{Au}_4$ catalyst. Spectra were collected immediately following the removal of the gas-phase CO: (a) 20 min at RT, (b) 25 min at RT, (c) 1 h at RT, (d) 20 min at 50°C , (e) 20 min at 80°C , (f) 20 min at 125°C , (g) 20 min at 150°C , (h) 20 min at 190°C .

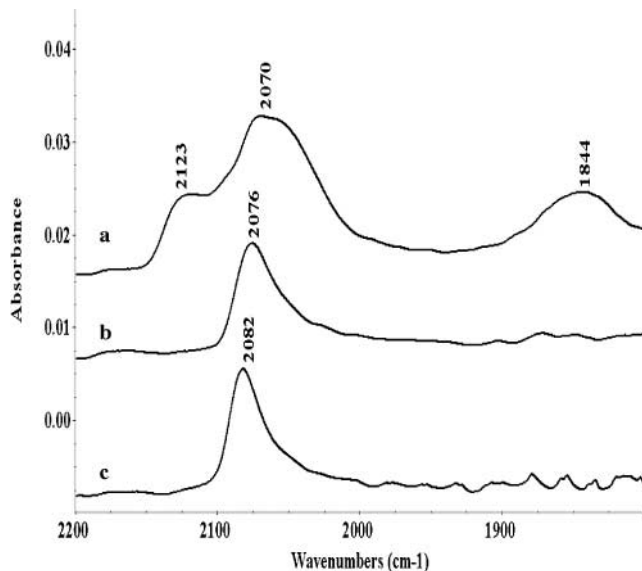


FIG. 5. IR spectra of adsorbed CO at RT (30°C) over SiO_2 -supported oxidized Pt and Pt–Au catalysts. Spectra were collected immediately following removal of the gas-phase CO: (a) $0.5\text{Pt}_2\text{Au}_4$, (b) 1Pt, (c) 1Pt–2Au.

Similar results to the ones obtained with the reduced samples were also observed with samples pretreated in oxygen. In this case, however, the CO stretching frequencies occur consistently at higher wave numbers. This could be due to either a compression of the CO layer caused by co-adsorbed oxygen, which predictably leads to higher frequencies than the ones obtained on reduced surfaces, or to an electronic effect associated with a weakening of the surface CO bond under these conditions (18). Spectra of the oxidized samples after exposure to CO at room temperature are shown in Fig. 5. Once again, a red shift of the Pt–CO peak and a new peak at 2123 cm^{-1} characteristic of Au-bound CO are evident in the spectrum of the $0.5\text{Pt}_2\text{Au}_4$ sample (Fig. 5, spectrum a). Furthermore, a new peak is identified in Fig. 5 (spectrum a) at 1844 cm^{-1} and can be assigned to bridge-bonded CO on Pt (19, 20).

FTIR studies of adsorbed CO were also conducted with the prereduced 1Pt, 1Pt–2Au, and $0.5\text{Pt}_2\text{Au}_4$ samples at elevated temperatures. Results of these studies are shown in Figs. 6 (for 1Pt) and 7 (for $0.5\text{Pt}_2\text{Au}_4$). The results obtained for the 1Pt–2Au are identical to those obtained with 1Pt and have not been included for brevity. In all cases, when the temperature was increased in the presence of gas-phase CO while the surface was allowed to equilibrate, the vibration frequency of adsorbed CO was noticeably decreased. It was also noticed that total CO desorption from Pt sites in the cluster-derived $0.5\text{Pt}_2\text{Au}_4$ catalyst occurs at higher temperatures than from the monometallic 1Pt sample. This suggests that on the average the CO–Pt bond is stronger in the cluster-derived catalyst (i.e., the fraction of lower coordination Pt sites is higher in this sample). This result is consistent with the substantial asymmetric tailing in the

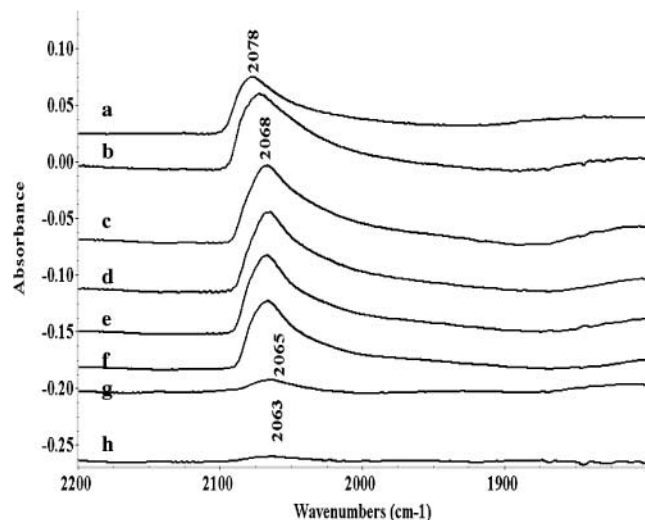


FIG. 6. FTIR spectra of adsorbed CO on reduced 1Pt collected in the presence of gas-phase CO at different temperatures: (a) RT, (b) 70°C, (c) 105°C, (d) 145°C, (e) 175°C, (f) 204°C, (g) 220°C, and (h) 245°C.

low-frequency region of the CO–Pt peak, which was discussed in a previous paragraph. Furthermore, the results of Figs. 6 and 7 suggest that the observed red shift at room temperature (i.e., full coverage) between CO adsorbed on Pt sites on 1Pt (or 1Pt–2Au) and 0.5Pt₂Au₄ may be related to differences in the singleton frequency of the adsorbed CO on these samples, since at the corresponding highest temperatures (i.e., lowest CO coverage) this red shift is further enhanced (from 2063 cm⁻¹ for 1Pt and 1Pt–2Au to 2049 cm⁻¹ for 0.5Pt₂Au₄). Finally, no significant shift was observed at elevated temperatures with the CO–Au band,

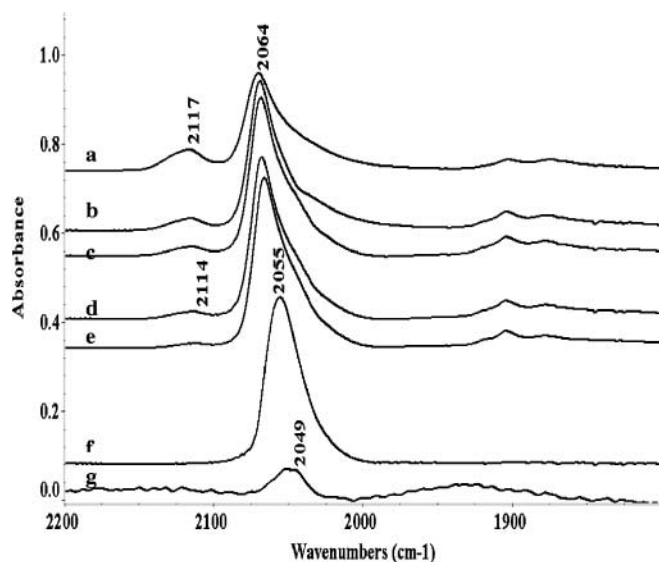


FIG. 7. FTIR spectra of adsorbed CO on reduced 0.5Pt₂Au₄ collected in the presence of gas-phase CO at different temperatures: (a) RT, (b) 60°C, (c) 70°C, (d) 85°C, (e) 110°C, (f) 249°C, and (g) 275°C.

indicating minimal coverage effects in this case. The clear difference in the magnitude of the shifts of the CO–Au and CO–Pt bands is another indication that the two bands are uncoupled and belong to different species. It is worth noting that previous room-temperature studies of the adsorption of CO on monometallic Au/SiO₂ catalysts indicate a blue shift with decreasing CO pressure (15, 21–23).

These results appear to suggest that the role of Au in the cluster-derived catalyst is beyond that of simply breaking up large Pt ensembles, and that Au may be electronically modifying the properties of Pt. However, due to the possibility of islands of CO formation even at low surface coverages (24), in which situation the dipole–dipole coupling is not completely eliminated, this hypothesis was further verified by collecting spectra of adsorbed ¹²CO/¹³CO mixtures at different ratios between the two isotopes. The dilution of one isotope in the other and the subsequent extrapolation of the observed frequencies to zero coverage yields another estimate of the singleton frequency. The frequency of ¹³CO–Pt was used in these calculations, because of interference between the frequency of ¹²CO–Pt and that of ¹³CO–Au (at approximately 2064 cm⁻¹) in the 0.5Pt₂Au₄ sample.

The IR spectra collected with different mixtures of adsorbed ¹²CO/¹³CO on pre-reduced 1Pt are shown in Fig. 8. The intensities associated with the two bands do not necessarily correspond to the ratio of the two isotopes in the mixture, since a transfer of intensity from one band to the other is possible, as was discussed previously by Toolenaar *et al.* (25) for Pt–Cu alloys. For the same reason, spectra collection at molar fractions above 4:1 or below 1:4 was virtually impossible. The spectra were deconvoluted using curve-fitting software packages, and peak

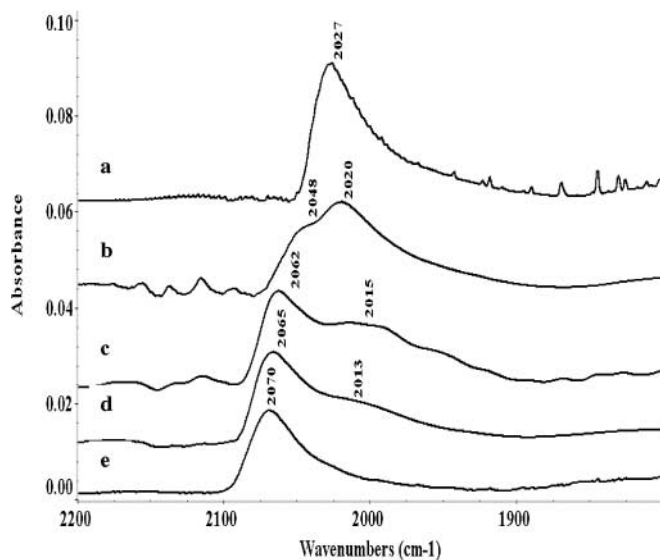


FIG. 8. RT spectra of mixtures of ¹²CO/¹³CO adsorbed on pre-reduced 1Pt: (a) 100% ¹³CO, (b) 35% ¹²CO/65% ¹³CO, (c) 50% ¹²CO/50% ¹³CO, (d) 65% ¹²CO/35% ¹³CO, and (e) 100% ¹²CO.

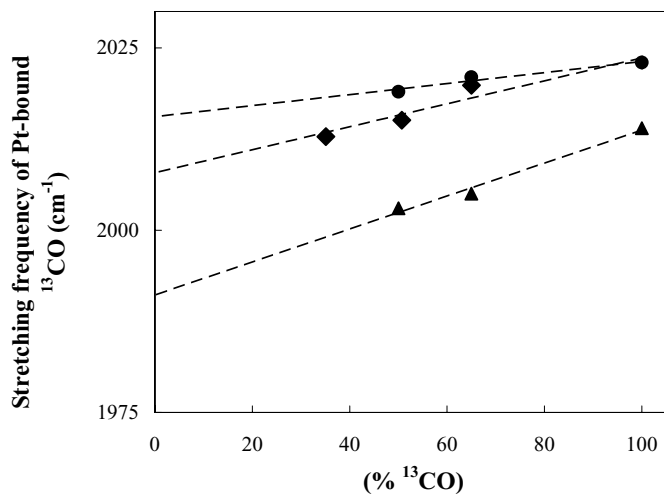


FIG. 9. RT stretching frequency of Pt-bound ^{13}CO adsorbed on different Pt and Pt–Au catalysts as a function of the molar fraction of ^{13}CO in the $^{12}\text{CO}/^{13}\text{CO}$ mixture: \blacklozenge , 1Pt; \bullet , 1Pt–2Au; \blacktriangle , 0.5Pt $_2$ Au $_4$.

positions of ^{13}CO were thus extracted. Plots of the frequency of adsorbed ^{13}CO on Pt obtained from this deconvolution procedure versus the ^{13}CO mole fraction in the $^{12}\text{CO}/^{13}\text{CO}$ mixture for the three catalysts examined are shown in Fig. 9. Extrapolation to zero concentration of ^{13}CO in the gas phase yields the ^{13}CO singleton frequency at full coverage, eliminating the dipole–dipole interactions between neighboring adsorbate molecules. These frequencies are shown in Table 2. Similar values were obtained for 1Pt and 1Pt–2Au (2008 and 2014 cm^{-1} , respectively), while a lower singleton frequency (1990 cm^{-1}) was obtained for the cluster-derived 0.5Pt $_2$ Au $_4$ sample, consistent with the results of the studies conducted at elevated temperatures. The combination of the two results suggests that in the case of the cluster-derived catalyst the electronic properties of Pt have been modified by the presence of Au.

3.3. Kinetic Results

3.3.1. Selective catalytic reduction of NO by propylene.

The NO reduction and propylene oxidation versus temperature curves for catalysts containing approximately 1 wt% Pt and for 2 wt% Au loadings are shown in Fig. 10. Identical results were obtained with the 1Pt and 1Pt–2Au samples.

TABLE 2

Singleton Frequencies Obtained from $^{12}\text{CO}/^{13}\text{CO}$ Experiments

Catalyst sample	Singleton frequency (cm^{-1})
1%Pt/SiO $_2$	2008
0.8%Pt–1.8%Au/SiO $_2$	2014
0.4%Pt $_2$ Au $_4$ /SiO $_2$	1990

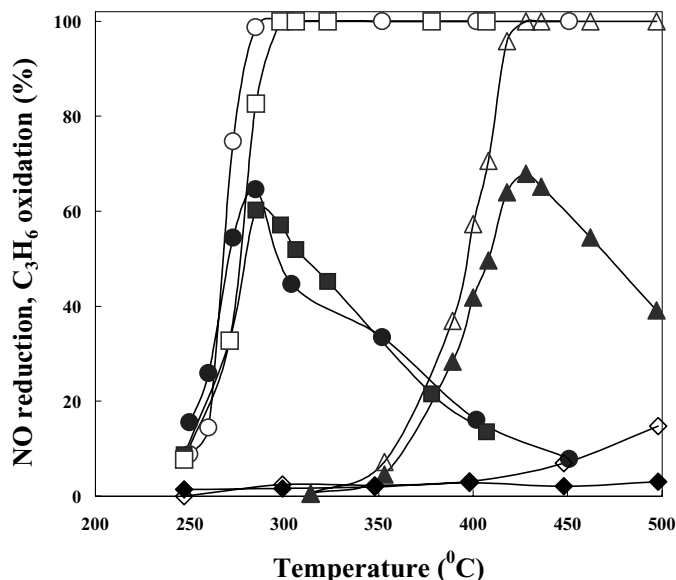


FIG. 10. NO reduction and C $_3$ H $_6$ oxidation vs. temperature over different SiO $_2$ -supported Pt and Pt–Au catalysts: \circ , \bullet , 1Pt; \square , \blacksquare , 1Pt–2Au; \triangle , \blacktriangle , 0.5Pt $_2$ Au $_4$; \diamond , \blacklozenge , 2Au. Open symbols: C $_3$ H $_6$ oxidation; closed symbols: NO reduction (1000 ppm NO, 1000 ppm C $_3$ H $_6$, 1% O $_2$, balance He, GHSV = 120,000 ml h $^{-1}$ g $^{-1}$).

In both cases, the NO reduction and propylene oxidation curves closely match each other up to the temperature of maximum NO reduction. At higher temperatures, the reduction of NO decreases, while the propylene oxidation reaches 100% and remains constant at this level. The selectivity toward N $_2$ in both cases ranges from 45 to 55%, consistent with what was previously observed with similar catalysts (26, 27).

A significantly different behavior was observed for the cluster-derived catalyst (0.5Pt $_2$ Au $_4$). In this case, a temperature delay of approximately 150°C was observed in both the NO reduction and propylene oxidation curves. In addition, a slight separation of the C $_3$ H $_6$ oxidation and NO reduction curves was observed, with C $_3$ H $_6$ oxidation preceding the NO reduction by approximately 10°C. Furthermore, the selectivity toward N $_2$ in this case was in the range of 70 to 80%, which is significantly higher than what was observed with the previous samples. Finally, the monometallic 2Au catalyst prepared by impregnation showed no activity toward NO reduction and only minor oxidation activity at temperatures above 450°C under the conditions studied.

A similar behavior was also observed for the oxidation of propylene in the absence of NO. Results of these studies are shown in Fig. 11. Once again, the performance of 1Pt and 1Pt–2Au was very similar with only a minor temperature delay of approximately 10°C observed in the light-off curve of the 1Pt–2Au sample. A significant shift of 150°C toward higher temperatures was observed with the cluster-derived catalyst, and the 2Au catalyst was only active at

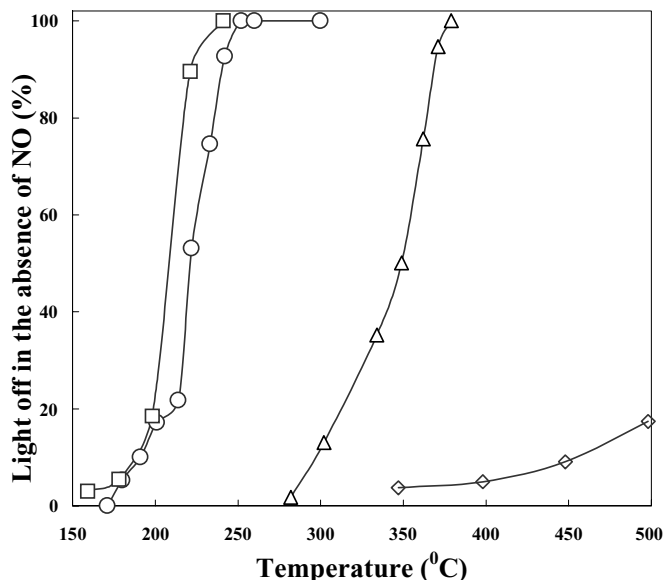


FIG. 11. C_3H_6 oxidation in the absence of NO vs. temperature over different SiO_2 -supported Pt and Pt–Au catalysts: \circ , 1Pt; \square , 1Pt–2Au; \triangle , 0.5Pt₂Au₄; \diamond , 2Au (1000 ppm C_3H_6 , 1% O_2 , balance He, GHSV = 120,000 ml h⁻¹ g⁻¹).

temperatures above 400°C. These results are consistent with our previous mechanistic conclusions regarding the kinetic significance of the hydrocarbon activation during HC-SCR at temperatures below the temperature of maximum NO reduction (28). In fact, the light-off curves of Fig. 11 indicate that the observed shift in the NO reduction profile for the cluster-derived catalyst under HC-SCR conditions can be directly attributed to the lower propylene oxidation activity of this catalyst. In contrast, the presence of Au in the co-impregnated sample does not have such an effect.

Similar experiments were also conducted over a series of catalysts with a nominal Pt loading of 0.15 wt%. As explained in the experimental section, the experiments in these cases were conducted at a proportionally lower space velocity (20,000 ml h⁻¹ g⁻¹) to facilitate comparisons among different catalyst samples. A small temperature delay (i.e., 20–25°C) in both the NO reduction and C_3H_6 oxidation curves was observed with the co-impregnated 0.15Pt–0.3Au sample compared to the monometallic 0.15Pt sample at temperatures below the temperature of the maximum NO reduction (Fig. 12). The selectivity toward N_2 was approximately 50%, and the magnitude of the maximum NO reduction was comparable in both cases. Once again, the 0.075Pt₂Au₄ cluster-derived catalyst exhibited a significant shift toward higher temperatures in both the NO reduction and the C_3H_6 oxidation profiles. As with the 0.5Pt₂Au₄ cluster-derived sample, the selectivity toward N_2 was also in the range of 70 to 80% in this case. A similar temperature shift was observed with the propylene oxidation in

the absence of NO. Finally, we should point out that the results of kinetic studies conducted with a monometallic 0.15Pt catalyst prepared using an organometallic *tert*-butyl ligated Pt cluster (10) indicate that the catalytic behavior of this material is identical to that of the monometallic 1Pt sample.

Previous studies have led to the conclusion that the oxidation of hydrocarbons over Pt is a structure-sensitive reaction. Carballo and Wolf (29), for example, reported that propylene oxidation over alumina-supported Pt proceeds at a significantly lower rate on smaller Pt particles. In that study, differences of 10 nm in particle size (i.e., for 1 to 11 nm) resulted in a ten-fold increase in the turnover frequency. Similar results were also reported by Garetto and Apestegua for the oxidation of cyclopentane, methane, and benzene (30, 31). A similar Pt particle size effect has also been reported for the selective reduction of NO by hydrocarbons. Lower turnover frequencies over smaller Pt crystallites have been observed, for example, for the reduction of NO by either propylene (32, 33) or octane (34). Furthermore, previous attempts to promote the catalytic activity of Pt for the selective catalytic reduction of NO by propylene by the addition of Au appear at first to have had contradictory results. Bimetallic Pt–Au catalysts prepared by incipient wetness impregnation from individual metal salts (35) or by redox techniques (36) have similar activity with the monometallic Pt only catalysts, in agreement with the results of this study. In contrast, reports from the patent

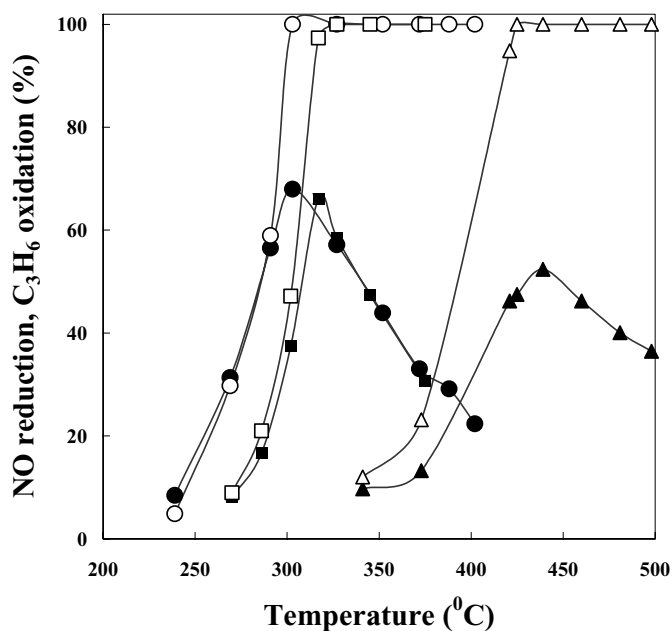


FIG. 12. NO reduction and C_3H_6 oxidation vs. temperature over different SiO_2 -supported Pt and Pt–Au catalysts: \circ , \bullet , 0.15Pt; \square , \blacksquare , 0.15Pt–0.3Au; \triangle , \blacktriangle , 0.075Pt₂Au₄; open symbols: C_3H_6 oxidation; closed symbols: NO reduction (1000 ppm NO, 1000 ppm C_3H_6 , 1% O_2 , balance He, GHSV = 20,000 ml h⁻¹ g⁻¹).

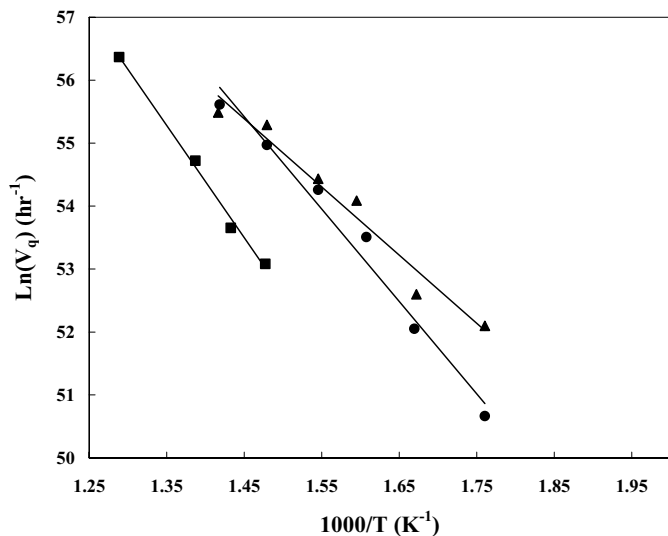


FIG. 13. Arrhenius plot for the $^{16}\text{O}/^{18}\text{O}$ homoexchange reaction: ▲, 1Pt; ●, 1Pt–2Au; ■, $0.5\text{Pt}_2\text{Au}_4$.

literature indicate a promoting effect when the Au was added by ion exchange or deposition methods (37).

In light of these reports, the results obtained in our study suggest the possibility of similar Pt particle or ensemble (in the case of the bimetallic catalysts) sizes for the monometallic Pt/SiO₂ and the co-impregnated Pt–Au/SiO₂ samples, and a significantly smaller Pt particle or ensemble size for the cluster-derived Pt₂Au₄/SiO₂ catalysts.

3.3.2. $^{16}\text{O}/^{18}\text{O}$ exchange reaction. Arrhenius plots (utilizing TOFs) for the $^{16}\text{O}/^{18}\text{O}$ exchange reaction over 1Pt, 1Pt–2Au, and $0.5\text{Pt}_2\text{Au}_4$ catalysts are shown in Fig. 13. The results indicate that the cluster-derived $0.5\text{Pt}_2\text{Au}_4$ sample is less active for the homoexchange reaction than the 1Pt or the 1Pt–2Au catalysts. The 1Pt and 1Pt–2Au samples exhibited similar activities. Finally, the 2Au sample was found to be completely inactive for this reaction, consistent with the idea that oxygen cannot be activated by gold. Apparent activation energies for the $^{16}\text{O}/^{18}\text{O}$ exchange reaction were calculated for the different samples from the slopes of the respective curves and the results are summarized in Table 3. A significantly higher apparent activation energy was observed over the cluster-derived sample.

TABLE 3

Apparent Activation Energy for the $^{16}\text{O}/^{18}\text{O}$ Homoexchange Reaction over Different SiO₂-Supported Pt and Pt–Au Samples

Catalyst sample	E_a (kJ/mol)
1Pt	90
1Pt–2Au	122
$0.5\text{Pt}_2\text{Au}_4$	148

It was previously shown that the $^{16}\text{O}/^{18}\text{O}$ homoexchange reaction over supported Pt catalysts is a structure-sensitive reaction favored over larger Pt particles or ensembles (38–40). In light of this previous work, our results suggest that in the case of the cluster-derived $0.5\text{Pt}_2\text{Au}_4$ catalyst the Pt ensembles are smaller than in the case of the 1Pt or the 1Pt–2Au samples prepared by impregnation. The 1Pt and 1Pt–2Au samples appear to have similar Pt particle or ensemble sizes. From this point of view, the results from the $^{16}\text{O}/^{18}\text{O}$ exchange reaction are in complete agreement with the results of the selective catalytic reduction of NO by propylene described in the previous section.

4. DISCUSSION

Kinetic results obtained for the selective catalytic reduction of NO by propylene, the oxidation of propylene in the absence of NO, and the $^{16}\text{O}/^{18}\text{O}$ homoexchange reaction indicate significant differences in the behavior of the various SiO₂-supported Pt and Pt–Au catalysts examined in this study. In particular, the cluster-derived $0.5\text{Pt}_2\text{Au}_4$ catalyst shows a significantly lower activity for all three reactions, which is manifested in the case of the HC-SCR and the propylene oxidation as a shift of the conversion-temperature curves toward higher temperatures. In addition, a higher selectivity for N₂ is observed with this catalyst during HC-SCR. In contrast, the 1Pt–2Au catalyst prepared by co-impregnation from individual precursors of Pt and Au exhibits behavior which is almost identical to that of the monometallic 1Pt catalyst. Corroborated with the fact that the monometallic 2Au catalyst prepared by impregnation is inactive for all three reactions, these results demonstrate that while Pt and Au do not affect each other in the 1Pt–2Au system, the presence of Au has a strong effect on the catalytic behavior of Pt in the cluster-derived $0.5\text{Pt}_2\text{Au}_4$ catalyst.

During the presentation of the results it was indicated that both the oxidation of hydrocarbons and the $^{16}\text{O}/^{18}\text{O}$ homoexchange reactions are known to be structure sensitive over supported platinum catalysts. In fact, the origin of the structure sensitivity is the same in both cases and is associated with the higher rate of the activation of molecular oxygen over larger Pt ensembles. Our previous work in the HC-SCR area has concluded that the activation of propylene by molecular oxygen is the rate-determining step of this reaction at temperatures below the temperature of maximum NO conversion (28, 41). Consequently, it is not surprising for HC-SCR to exhibit the same type of structure sensitivity as well. In fact, there are published literature reports that have experimentally demonstrated such a structured sensitivity effect over supported Pt catalysts with different Pt particle sizes (33, 34). Hence, in light of these reports, it is reasonable to attempt to attribute the differences in the kinetic results obtained in this study to

differences in Pt ensemble sizes and, in particular, to a smaller Pt ensemble size in the case of the cluster-derived $0.5\text{Pt}_2\text{Au}_4$ catalyst.

Indeed, the results of the TEM and hydrogen chemisorption measurements suggest that the cluster-derived catalyst has a slightly smaller metal particle size (on the order of 1 nm) and a higher Pt dispersion than either the monometallic 1Pt or the co-impregnated 1Pt–2Au systems. However, given the magnitude of the structure sensitivity effects reported previously for the reactions examined (33, 34, 39, 40), it becomes clear that these differences in metal particle size are not sufficient to justify the observed differences in catalytic behavior. As mentioned in the previous paragraph, the kinetic results suggest that the active Pt ensemble size in the cluster-derived $0.5\text{Pt}_2\text{Au}_4$ catalyst is significantly smaller than the active Pt ensemble size in the monometallic 1Pt and the co-impregnated 1Pt–2Au systems. Since identical kinetic results were obtained with the monometallic Pt catalysts irrespective of the precursor used (salt-derived or cluster-derived) as was discussed in section 3.3.1, the smaller Pt ensemble sizes in the former case can be attributed to the presence of Au. In turn, this can be interpreted as the first indication of the formation of Pt–Au bimetallic particles in the $0.5\text{Pt}_2\text{Au}_4$ catalyst. The presence of Au in the surface of such particles is expected to “break down” large Pt ensembles and result in an average Pt ensemble size, which is significantly smaller than the average metal particle size. In addition, it is possible that the presence of Au in such bimetallic particles also results in a modification of the electronic, and hence catalytic, properties of Pt.

Further evidence for the formation of Pt–Au bimetallic particles in the $0.5\text{Pt}_2\text{Au}_4$ catalyst can be found in the results of the CO adsorption experiments conducted in this study. The FTIR spectra of this catalyst collected at room temperature and full CO coverage indicate the presence of a new Au-bound weakly adsorbed surface CO species and a red shift in the frequency of the Pt-bound CO. Previous literature reports indicate that only finely dispersed Au crystallites lower than 5 nm in diameter can adsorb CO. Therefore, the FTIR results suggest that Au is finely dispersed in this sample. The red shift observed in the same FTIR spectra in the frequency of the Pt-bound CO can be associated with either a geometric or an electronic effect. In the first case, the geometric (“dilution”) effect is the result of Au breaking up the large Pt ensembles, thus creating a weaker lateral interaction between adsorbed CO molecules (i.e., decreased dipole–dipole coupling in the adlayer). In the second case, electronic donation from one metal to the other can increase the back donation in the $2\pi^*$ antibonding orbitals of adsorbed CO molecules, and consequently cause the observed red shift. The estimation of the singleton frequency (i.e., the frequency of a single CO molecule adsorbed on one metal site) can help to dis-

cern between dipole–dipole coupling shifts and shifts due to changes in the electronic state of the surface metal site. Such estimates were obtained by two different approaches: surface equilibration with gas-phase CO at elevated temperatures (i.e., equilibrated low surface coverages of CO) and use of $^{12}\text{CO}/^{13}\text{CO}$ mixtures at full coverage. Although at first it appears that both approaches provide the same result, in reality two different values of the singleton frequency can be obtained. The high-temperature experiments reveal the frequency of a single CO molecule adsorbed on a practically empty surface, while the experiments utilizing mixtures of the two isotopes reveal the frequency of an uncoupled ^{12}CO (or ^{13}CO) molecule adsorbed on a surface saturated with ^{13}CO (or ^{12}CO) molecules.

The important point from the perspective of this paper is that both approaches demonstrated differences of about $15\text{--}20\text{ cm}^{-1}$ in the singleton frequency of adsorbed CO on the cluster-derived $0.5\text{Pt}_2\text{Au}_4$ catalyst, compared to the monometallic 1Pt catalyst or the 1Pt–2Au catalyst prepared by co-impregnation from individual precursors of Pt and Au. These differences are a clear indication that in the cluster-derived catalyst not only the Pt ensemble size has been affected, but also the electronic properties of Pt have been modified by the presence of Au. Hence, the combination of kinetic and spectroscopic evidence leads to the conclusion that in the cluster-derived catalyst Pt and Au are intimately mixed in the form of bimetallic Pt–Au particles. These particles are much larger than the original six metal atom clusters and, therefore, agglomeration is taking place during the ligand-removal process. However, it appears that during this agglomeration no significant segregation of Pt and Au takes place.

The formation of bimetallic particles is greatly dependent on the precursors used. In contrast to the cluster-derived catalyst, the 1Pt–2Au catalyst prepared by co-impregnation from individual precursors of Pt and Au exhibits both catalytic and spectroscopic properties that are very similar to those of the monometallic 1Pt sample. This material appears to follow a model in which Pt and Au are segregated, which would be expected based on the miscibility gap between the two metals. Furthermore, Au in this material appears to be in the form of larger crystallites since the FTIR studies did not reveal any CO adsorption. In fact, it is reasonable to assume that the majority of Au is in the form of the larger particles observed in the tail end of the metal particle size distribution of this catalyst (Fig. 1).

Finally, we should point out that although the use of the organometallic Pt–Au cluster precursors appears to prevent the segregation of the two metals into separate particles, metal mobility within these particles and the subsequent surface-enrichment effect cannot be ruled out. Thermodynamic arguments indicate that the surface of the bimetallic particles is expected to be enriched with the element having the lowest surface tension. In the Pt–Au pair, Au exhibits

the lowest surface tension and therefore a Au enrichment of the surface is possible. However, a lower hydrogen uptake would be expected if the surface was enriched in Au, and no such trend was observed in the data of Table 1. This may be due to the nanoscale dimension of the bimetallic particles involved in this study. At this scale, metal behavior may differ significantly from “bulk” behavior observed with larger particles.

5. CONCLUSIONS

The use of an acetylide-ligated organometallic Pt–Au cluster as a precursor has led to the synthesis of supported Pt–Au catalysts containing bimetallic Pt–Au particles. In contrast, a conventional synthesis approach utilizing incipient wetness impregnation of individual Pt and Au precursors results in catalysts containing segregated Pt and Au catalysts. Catalysts prepared using the cluster route exhibited significantly different catalytic behavior for a series of test reactions, in addition to different adsorption properties for CO. These differences are the result of the presence of finely dispersed Au, smaller Pt ensembles, and modification of the electronic properties of Pt by Au in the Pt–Au bimetallic particles. These particles appear to be fairly stable and retain their properties and composition even after prolonged exposure to HC-SCR conditions (i.e., oxidative atmosphere and temperatures up to 500°C).

ACKNOWLEDGMENTS

The authors express their gratitude to the U.S. Department of Energy (DE-FG02-96ER14666) for financial support of this work. M. D. A. also acknowledges support from an international supplement from the National Science Foundation (CTS-9624433). Finally, Bert D. Chandler is acknowledged for the preparation of the organometallic clusters used as precursors and for his useful suggestions during this work.

REFERENCES

- Bouwman, R., and Sachtler, W. H. M., *J. Catal.* **19**, 127 (1970).
- Sachdev, A., and Schwank, J., *J. Catal.* **120**, 353 (1989).
- Gates, B. C., *Chem. Rev.* **95**, 511 (1995).
- Psaro, R., and Recchia, S., *Catal. Today* **41**, 139 (1998).
- Graf, I. V. G., Bacon, J. W., Curley, M. E., Ito, L. N., and Pignolet, L. H., *Inorg. Chem.* **35**, 689 (1996).
- Chandler, B. D., Rubinstein, L. I., and Pignolet, L. H., *J. Mol. Catal.* **133**, 267 (1998).
- Chandler, B. D., Schabel, A. B., Blanford, F., and Pignolet, L. H., *J. Catal.* **187**, 367 (1999).
- Chandler, B. D., and Pignolet, L. H., *Catal. Today* **65**, 39 (2001).
- Chandler, B. D., Schabel, A. B., and Pignolet, L. H., *J. Phys. Chem. B* **105**, 149 (2001).
- Chandler, B. D., Ph.D. dissertation, University of Minnesota, Minneapolis, 1999.
- Espinet, P., Fornies, J., Martinez, F., Tomas, M., Lalinde, E., Moreno, M. T., Ruiz, A., and Welch, A. J., *J. Chem. Soc., Dalton Trans.* 791 (1990).
- Martin, D., and Duprez, D., *J. Phys. Chem.* **100**, 9429 (1996).
- Balakrishnan, K., Sachdev, A., and Schwank, J., *J. Catal.* **121**, 441 (1990).
- Schwank, J., Balakrishnan, K., Sachdev, A., Volter, J., Ryczkowski, J., Figueras, F., Grunert, W., Menon, P. G., Clarke, J. K. A., Coenen, J., and Paffett, M., *Stud. Surf. Sci. Catal.* **75**, 905 (1993).
- Yates, D. J. C., *J. Colloid Interface Sci.* **29**, 194 (1969).
- Boccuzzi, F., Guglielminotti, E., Pinna, F., and Strukul, G., *Surf. Sci.* **377**, 728 (1997).
- Liu, H., Kozlov, A. I., Kozlova, A. P., Shido, T., Asakura, K., and Iwasawa, Y., *J. Catal.* **185**, 252 (1999).
- Conrad, H., Ertl, G., and Kuppers, J., *Surf. Sci.* **76**, 323 (1978).
- Delacruz, C., and Sheppard, N., *Spectrochim. Acta Part A* **50**, 271 (1994).
- Podkolzin, S. G., Shen, J., de Pablo, J. J., and Dumesic, J. A., *J. Phys. Chem. B* **104**, 4169 (2000).
- France, J., and Hollins, P., *J. Electron Spectrosc. Relat. Phenom.* **64/65**, 251 (1993).
- Schubert, M. M., Kahlich, M. J., Gasteiger, H. A., and Behm, R. J., *J. Power Sources* **84**, 175 (1999).
- Boccuzzi, F., Chiorino, A., Tsubota, S., and Haruta, M., *J. Phys. Chem.* **100**, 3625 (1996).
- Crossley, A., and King, D. A., *Surf. Sci.* **95**, 131 (1980).
- Toolenaar, F. J. C., Stoop, F., and Ponc, V., *J. Catal.* **82**, 1 (1983).
- Roberts, K. L., and Amiridis, M. D., *Ind. Eng. Chem. Res.* **36**, 3528 (1997).
- Captain, D. K., Roberts, K. L., and Amiridis, M. D., *Catal. Today* **42**, 93 (1998).
- Captain, D. K., Mihut, C., Dumesic, J. A., and Amiridis, M. D., *Catal. Lett.*, submitted for publication.
- Carballo, L. M., and Wolf, E. E., *J. Catal.* **53**, 366 (1978).
- Garetto, T. F., and Apesteguia, C. R., *Catal. Today* **62**, 189 (2000).
- Garetto, T. F., and Apesteguia, C. R., *Appl. Catal. B* **32**, 83 (2000).
- Lee, J.-H., and Kung, H. H., *Catal. Lett.* **51**, 1 (1998).
- Denton, P., Giroir-Fendler, A., Praliaud, H., and Primet, M., *J. Catal.* **189**, 410 (2000).
- Burch, R., Fornasiero, P., and Southward, B. W. L., *Chem. Commun.* 625 (1998).
- Burch, R., and Watling, T. C., *Appl. Catal. B* **11**, 207 (1997).
- Demichelli, M. C., Hoang, L. C., Menezes, J. C., Barbier, J., and Pinabiau-Carlier, M., *Appl. Catal. A* **97**, L11 (1993).
- Nakatsuji, T., EP 0 602 602 A1 (1993).
- Taha, R., and Duprez, D., *J. Chim. Phys.* **92**, 1506 (1995).
- Duprez, D., *Stud. Surf. Sci. Catal.* **112**, 13 (1997).
- Descorme, C., and Duprez, D., *Appl. Catal. A* **202**, 231 (2000).
- Captain, D. K., and Amiridis, M. D., *J. Catal.* **194**, 222 (2000).